Title

Terminal NiII−OH/−OH2 complexes in trigonal bipyramidal geometries derived from H2O

Authors

Lau, Nathanael
Sano, Yohei
Ziller, Joseph W
et al.

Publication Date

2017-03-01

DOI

10.1016/j.poly.2016.11.015

Peer reviewed

HHS Public Access

Author manuscript

Polyhedron. Author manuscript; available in PMC 2018 March 29.

Published in final edited form as:

Polyhedron. 2017 March 29; 125: 179–185. doi:10.1016/j.poly.2016.11.015.

Terminal Ni^{II}–OH/–OH_2 complexes in trigonal bipyramidal geometries derived from H_2O

Nathanael Lau, **Yohei Sano**, **Joseph W. Ziller**, and **A.S. Borovik**

Department of Chemistry, University of California – Irvine, 1102 Natural Sciences II, Irvine, CA 92697-2025, United States

Abstract

The preparation and characterization of two Ni^{II} complexes are described, a terminal Ni^{II}–OH complex with the tripodal ligand tris[(N)-tertbutylureaylato)-N-ethyl)]aminato ($[H_3buea]^{3-}$) and a terminal Ni ^{II}–OH_2 complex with the tripodal ligand *N*,*N*′,*N*″-[2,2′,2″-nitrilotris(ethane-2,1-diyl)]tris(2,4,6-trimethylbenzenesulfonamido) ($[MST]^{3-}$). For both complexes, the source of the –OH and –OH_2 ligand is water. The salts $K_2[Ni^{II}H_3buea(OH)]$ and $NMe_4[Ni^{II}MST(OH_2)]$ were characterized using perpendicular-mode X-band electronic paramagnetic resonance, Fourier transform infrared, UV-visible spectroscopies, and its electrochemical properties were evaluated using cyclic voltammetry. The solid state structures of these complexes determined by X-ray diffraction methods reveal that they adopt a distorted trigonal bipyramidal geometry, an unusual structure for 5-coordinate Ni^{II} complexes. Moreover, the Ni^{II}–OH and Ni^{II}–OH_2 units form intramolecular hydrogen bonding networks with the $[H_3buea]^{3-}$ and $[MST]^{3-}$ ligands. The oxidation chemistry of these complexes was explored by treating the high-spin Ni^{II} compounds with one-electron oxidants. Species were formed with S = 1/2 spin ground states that are consistent with formation of monomeric Ni^{III} species. While the formation of Ni^{III}–OH complexes cannot be ruled out, the lack of observable O-H vibrations from the putative Ni–OH units suggest the possibility that other high valent Ni species are formed.

Graphical Abstract

A terminal Ni^{II}–OH complex and a terminal Ni^{II}–OH_2 complex, both supported by tripodal ligands, have been prepared and characterized. The solid state structures of these complexes reveal that they adopt distorted trigonal bipyramidal primary coordination spheres, an unusual geometry for Ni^{II} complexes. Treating these complexes with one-electron oxidants formed species with S = 1/2 spin ground states, which are consistent with formation of monomeric Ni^{III} species.

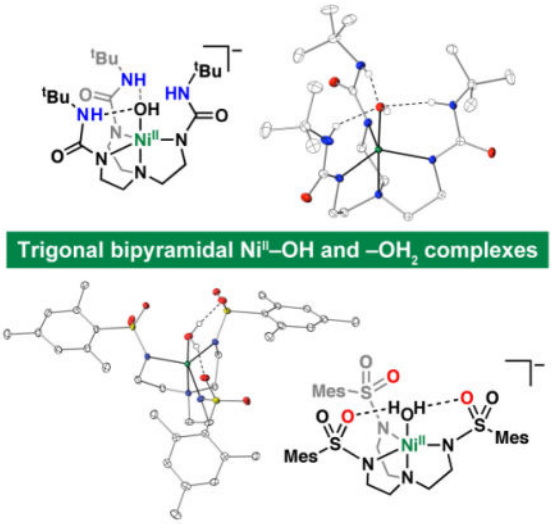

Keywords

Nickel-hydroxido complexes; Nickel-aqua complexes

1. Introduction

Monomeric metal complexes of first-row transition metal ions with terminal hydroxido and aqua ligands are often difficult to prepare because of the strong tendency of these ligands to bridge between metal centers [1–10]. However, hydroxido and aqua bridging may be prevented by using steric effects, as evidenced by the ubiquity of terminal metal hydroxido and aqua units in biology [11–15]. Using steric effects in this manner is also effective in synthetic systems, as most synthetic terminal nickel hydroxido and aqua complexes use sterically encumbered ligand frameworks around the metal center to prevent bridging. Cámpora prepared the earliest examples of monomeric square planar terminal Ni^{II}–OH moieties [16,17], and a number of similar 4-coordinate terminal Ni^{II}–OH complexes have been developed for catalysis [18–21]. To the best of our knowledge, there are only two examples of crystallographically characterized monometallic 5-coordinate Ni^{II}–OH complexes. Riordan has prepared a square pyramidal complex with a 1,4,8,11-tetramethyl-1,4,8,11-tetraazadodecane ligand in which the exogenous hydroxido ligand is derived from dioxygen [22], and Levy has prepared a trigonal bipyramidal complex with a bulky Schiff base ligand where the exogenous hydroxido ligand is derived from adventitious water [23]. The earliest structurally characterized 5-coordinate terminal Ni^{II}–OH$_2$ complex was reported by Stuky in 1969 [24], and since then many other structurally characterized terminal Ni^{II}–OH$_2$ complexes have been prepared [25–27].

Our group has also successfully used this approach to prepare many terminal metal hydroxido and aqua complexes, including a pair of terminal Ni^{II}–OH complexes using sterically bulky tridentate ligands [28]. The ligands used in that work were derived from the urea based tripodal ligand tris[(N)-tertbutylureaylato)-N-ethyl)] aminato ([H$_3$buea]$^{3-}$),

shown in Fig. 1A [29]. Various monometallic terminal metal hydroxido and oxido complexes have been stabilized with $[H_3buea]^{3-}$, as the three *tert*-butyl groups of $[H_3buea]^{3-}$ protects the hydroxido or oxido ligand by hindering access [30–32]. An additional feature of $[H_3buea]^{3-}$ is its ability to promote the formation of intramolecular hydrogen bonds (H-bonds). For instance, in our previously prepared M–OH complexes the terminal hydroxido ligand was further stabilized through intramolecular H-bonding networks that are formed between the urea N–H groups of $[H_3buea]^{3-}$ and the oxygen atom of the hydroxido ligand.

Our group has also designed systems that are capable of accepting H-bonds from an apical exogenous ligand. For example, the ligand *N*,*N*′,*N*″-[2,2′,2″-nitrilotris(ethane-2,1-diyl)]tris(2,4,6-trimethylbenzenesulfonamido) ($[MST]^{3-}$) (Fig. 1B) is a sulfonamide-based tripodal ligand that can stabilize hydroxido or aqua ligands through intramolecular H-bonds involving the O–H group and the sulfonamido oxygen atoms [33–35]. In addition, the S=O and mesityl groups in $[MST]^{3-}$ appear to be bulky enough to help prevent the hydroxido or aqua ligand from bridging [36–38].

The following work describes the synthesis and characterization of a Ni^{II}–OH complex with the ligand $[H_3buea]^{3-}$ and a Ni^{II}–OH_2 complex with the ligand $[MST]^{3-}$, where the hydroxido and aqua ligands were both derived from water. Our previous work suggested to us that these ligands would be logical candidates to stabilize monomeric Ni^{II} complexes with terminal hydroxido and aqua ligands. We also probed their oxidative chemistry with the goal of establishing the properties of Ni^{III}–OH species. Such species are believed to be a key intermediate in Ni based oxidations [39–43], but to date, no putative Ni^{III}–OH species has been structurally characterized. Our findings show that while new oxidize species can be detected, our evidence does not conclusive show that the Ni^{III}–OH unit has remained intact.

2. Experimental

2.1. General Methods

All reagents were purchased from commercial sources and used as received, unless otherwise noted. Solvents were sparged with argon and dried over columns containing Q-5 and molecular sieves. The tripodal compounds H_6buea and H_3MST were synthesized following literature procedures [29,33]. The preparations of metal complexes were conducted in a Vacuum Atmospheres, Co. drybox under argon atmosphere. Potassium hydride (KH) as a 60% dispersion in mineral oil was filtered with a medium porosity glass-fritted funnel and washed 5 times each with pentane and diethyl ether (Et_2O). Solid KH was dried under vacuum and stored under inert atmosphere. $Ni(OAc)_2$ was prepared by literature procedures [44]. I_2 was sublimed under vacuum and stored under inert atmosphere. Water was degassed by five freeze-pump-thaw cycles and stored under inert atmosphere.

2.2. Preparation of the complexes with $[H_3buea]^{3-}$

2.2.1. Preparation of $K_2[Ni^{II}H_3buea(OH)]$—A solution of H_6buea (300 mg, 0.69 mmol) in anhydrous dimethylacetamide (DMA) (20 mL) was treated with solid KH (110 mg, 2.9 mmol). The mixture was stirred until gas evolution ceased. $Ni(OAc)_2$ (120 mg, 0.69 mmol) was added to the clear pale yellow reaction mixture, and the solution was stirred. After 2 h,

H_2O (13 μL, 0.72 mmol) was added to the red solution *via* syringe, and the mixture was stirred for 15 min. After the addition of dimethylformamide (DMF) (4 mL), the reaction mixture was filtered through a medium porosity glass-fritted funnel to remove the insoluble KOAc. The green-yellow filtrate was concentrated under vacuum to *ca.* 1 mL and treated with Et_2O (20 mL) followed by pentane (20 mL) to precipitate a green solid. The green solid was collected on a fine porosity glass-fritted funnel and dried under vacuum. After 1 h, the solid was washed with acetonitrile (MeCN) to remove an orange filtrate. The green solid was redissolved in DMA (20 mL) and recrystallized by slow diffusion with Et_2O. After 2 d, green crystals were collected to give 360 mg (87%) of product. Elemental Anal. Calc. for $K_2[Ni^{II}H_3buea(OH)]\cdot 2DMF$, $K_2NiC_{29}H_{61}N_9O_6$: C, 45.31; H, 8.00; N, 16.40. Found: C, 45.01; H, 8.19; N, 16.15%. FTIR (KBr disc, cm^{-1}, selected bands): 3233, 3146, 2962, 2921, 2849, 1592, 1509, 1447, 1388, 1357, 1247, 1223, 1149, 1118, 1034, 971, 796, 731. λ_{max} (DMF, nm, ε $M^{-1}cm^{-1}$): 324 (1400), 424 (61), 493 (35), 677 (23). μ_{eff} (DMSO, μ_B): 3.1. E_a (DMF): −0.830 V versus $[FeCp_2]^{0/+}$.

2.2.2. Oxidation of $K_2[Ni^{II}H_3buea(OH)]$—A solution of $K_2[Ni^{II}H_3buea(OH)]$ (50 mg, 0.085 mmol) in DMF (2 mL) was treated with solid I_2 (11 mg, 0.045 mmol). The yellow-green solution immediately turned purple-red and was allowed to stir for 5 min. The solution was concentrated under vacuum until near dryness and Et_2O (5 mL) was added to precipitate a purple-red powder. After decanting the liquid, the powder was redissolved in THF (2 mL). The reaction mixture was filtered through a fine porosity glass-fritted funnel to remove the insoluble KI. The filtrate was concentrated under vacuum until near dryness then treated with Et_2O (5mL) and the resulting red powder was collected on a medium porosity glass-fritted funnel. EPR (DMF, 77 K): g = 2.29, 2.17, 2.04. FTIR (ATR, cm^{-1}, selected bands): 3308, 2958, 2888, 1587, 1474, 1451, 1386, 1351, 1259, 1223, 1151, 1103, 1032, 961, 837, 777, 754. λ_{max} (DMF, nm, ε $M^{-1}cm^{-1}$): 326 (~ 2000), 502 (~ 570).

2.3. Preparation of the complexes with $[MST]^{3-}$

2.3.1. Preparation of $NMe_4[Ni^{II}MST(OH_2)]$—A solution of H_3MST (205 mg, 0.30 mmol) in anhydrous DMA (4 mL) was treated with solid KH (37 mg, 0.91 mmol). The mixture was stirred until gas evolution ceased. $Ni(OAc)_2\cdot 4H_2O$ (73 mg, 0.29 mmol) and NMe_4OAc (40 mg, 0.30 mmol) were added to the clear pale yellow reaction, and the solution was stirred. After 3 h, Et_2O (5 mL) was added to the green-yellow solution to aid the precipitation of KOAc. The reaction mixture was filtered through a medium porosity glass-fritted funnel to remove the insoluble species. The filtrate was concentrated under vacuum to *ca.* 1 mL and treated with Et_2O (10 mL) followed by pentane (40 mL) to precipitate a yellow solid. The yellow solid was collected on a medium porosity glass-fritted funnel and dried under vacuum to give 207 mg (85%) of product. FTIR (KBr disc, cm^{-1}, selected bands): 3259, 3030, 2973, 2937, 2854, 1603, 1563, 1490, 1468, 1254, 1128, 1054, 977, 830, 815, 742, 656, 610. MS (ES-, m/z): Exact mass calcd for $NiC_{33}H_{45}N_4O_6S_3$: 747.2. Found: 747.2. This salt, presumably $NMe_4[Ni^{II}MST]$ (77 mg, 0.092 mmol) was redissolved in CH_2Cl_2 (10 mL) and treated with H_2O (2 μL, 0.10 mmol) in one portion *via* a syringe, and the mixture was stirred. After 15 min the green solution was filtered through a medium porosity glass-fritted funnel to remove any insoluble species and the filtrate was layered under pentane. After 2 d, green and yellow needle crystals were collected via filtration and

dried very briefly under vacuum, to give 74 mg (94%) of crystalline product. Elemental Anal. Calc. for $NMe_4[Ni^{II}MST(OH_2)]$ $NiC_{37}H_{59}N_5O_7S_3$: C, 52.86; H, 7.07; N, 8.33. Found: C, 52.95; H, 7.16; N, 8.18%. FTIR (KBr disc, cm^{-1}, selected bands): 3266, 3025, 2970, 2934, 2855, 1604, 1562, 1490, 1468, 1405, 1377, 1342, 1258, 1230, 1132, 1054, 977, 813, 742, 657, 607. (Nujol, cm^{-1}): 3241 (OH). (CH_2Cl_2, 20 mM, cm^{-1}): 3280. λ_{max} (DMF, nm, ε $M^{-1}cm^{-1}$): 312 (3300) 431 (120), 506 (39), 724 (33). μ_{eff} (μ_B): 3.22. $E_{1/2}$ (MeCN): 0.370 V versus $[FeCp_2]^{0/+}$

2.3.2. Preparation of tris-(4-bromophenyl)ammoniumyl hexafluorophosphate ([TBPA][PF_6])—[TBPA][PF_6] was prepared according to literature procedures with the following modifications [45,46]. A solution of tris-(4-bromophenyl)amine (200 mg, 0.42 mmol) in CH_2Cl_2 (2 mL) was cooled to −30 °C. Upon addition of nitrosonium hexafluorophosphate ([NO][PF_6], 74 mg, 0.41 mmol), the clear solution immediately became dark blue. After 1 h of stirring at −30 °C, pentane (20 mL) was added to precipitate a dark blue solid. The solid was collected by filtering through a medium porosity glass-fritted funnel, washed with pentane (20 mL), dried under vacuum to yield 211 mg (81%) dark blue powder, and stored at −30°C. EPR (CH_2Cl_2, 77 K): g = 2.00. λ_{max} (CH_2Cl_2, nm, ε $M^{-1}cm^{-1}$): 309 (6.4×10^4), 367 (7.2×10^4), 725 (1.1×10^5).

2.3.3. Oxidation of $NMe_4[Ni^{II}MST(OH_2)]$—A solution of $NMe_4[Ni^{II}MST(OH_2)]$ (25 mg, 0.030 mmol) in CH_2Cl_2 (2 mL) was cooled to −30°C, then treated with a solution of [TBPA][PF_6] (21 mg, 0.033 mmol) in CH_2Cl_2 (1 mL) at −30°C. The yellow-green solution immediately turned orange-red, and was allowed to stir at −30°C for 5 min. The solution was concentrated under vacuum until near dryness, washed with Et_2O (5mL), and collected on a medium porosity glass-fritted funnel. EPR (CH_2Cl_2, 77 K): g = 2.66, 2.15, 1.99. FTIR (ATR, cm^{-1}, selected bands): 3250, 3021, 2968, 2934, 2853, 1602, 1579, 1485, 1415, 1380, 1311, 1265, 1184, 1152, 1098, 1071, 1054, 1006, 976, 950, 830, 734, 654, 609. λ_{max} (CH_2Cl_2, nm, ε $M^{-1}cm^{-1}$): 312 (>12000), 440 (~1200) and 530 (~550)

2.4. Physical Methods

Elemental analyses were performed on a Perkin-Elmer 2400 CHNS analyzer. ^1H NMR and ^{13}C NMR were recorded on a Bruker DRX500 spectrometer. FTIR spectra were collected on a Varian 800 Scimitar Series FTIR spectrometer in air or a Thermo Scientific Nicolet iS5 spectrophotometer with an iD5 Attenuated Total Reflectance (ATR) attachment in a nitrogen filled glovebox. High-resolution mass spectra were collected using Waters Micromass LCT Premier Mass Spectrometer. UV-vis spectra were recorded with a Cary 50 or an Agilent 8453 spectrophotometer using a 1.00 cm quartz cuvette. Perpendicular-mode X-band EPR spectra were collected using a Bruker EMX spectrometer at 10K using liquid helium. Solution effective magnetic moments were measured by the Evans' method on a Bruker DRX500 spectrometer using flame sealed standard cores of 1:1 DMSO:DMSO-d_6 or 1:1 $CHCl_3$:$CDCl_3$.[47] Cyclic voltammetry (CV) experiments were conducted using a CH1600C electrochemical analyzer. A 2.0 mm glassy carbon electrode was used as the working electrode at scan velocities 0.5 Vs^{-1} unless otherwise noted. A cobaltocenium/cobaltocene couple ($[CoCp_2]^{+/0}$) was used as an internal reference then scaled against the

ferrocene/ferrocenium couple ($[FeCp_2]^{0/+}$).[48] Tetrabutylammonium hexafluorophosphate (TBAP) was use as the supporting electrolyte at a concentration of 0.1 M.

2.5. Crystallography

A Bruker SMART APEX II diffractometer and the APEX2 program package was used to determine the unit-cell parameters and for data collection. Crystallographic details are summarized in the Supporting information, and in Table S1.

3. Results and Discussion

3.1. Preparation and properties of $K_2[Ni^{II}H_3buea(OH)]$

The preparation of $K_2[Ni^{II}H_3buea(OH)]$ followed literature methods reported for other M^{II}–OH with $[H_3buea]^{3-}$ (Scheme 1) [49]. Green crystals of this salt suitable for X-ray diffraction were obtained by slow diffusion of Et_2O vapors into a DMA or DMF solution of the compound.

The absorbance spectrum of $[Ni^{II}H_3buea(OH)]^{2-}$ displayed peaks in the visible region at λ_{max} = 424 (ε = 61), 493 (ε = 35), and 677 nm (ε = 23). These absorbance features are similar to those of other Ni^{II} centers in local C_3 symmetry [50,51]. The X-band perpendicular-mode EPR spectrum taken at 77 K was silent, which is expected for a d_8 metal center of integer spin. Evans' method was used to determine the solution effective magnetic moment of 3.1 μ_B [47]. This value is consistent with the spin-only value for an S = 1 system of 2.8 μ_B, indicating that the Ni^{II} metal center is high-spin. The FTIR spectra of $K_2[Ni^{II}H_3buea(OH)]$, recorded both with ATR-IR and as a Nujol mull, did not show peaks corresponding to an O–H vibration from the hydroxido ligand. Note that all other M^{II}–OH complexes with $[H_3buea]^{3-}$ also fail to reveal any peaks for the ν(OH) [49]; the reason for the absence of these signals in not known.

3.2. Preparation and properties of $NMe_4[Ni^{II}MST(OH_2)]$

The preparation of $NMe_4[Ni^{II}MST(OH_2)]$ also followed a reported route from our group (Scheme 2) [38]. Green crystals of this salt suitable for X-ray diffraction were obtained by layering a CH_2Cl_2 solution of the compound under pentane.

The absorbance spectrum of $[Ni^{II}MST(OH_2)]^-$ was characterized by peaks in the visible region at λ_{max} = 431 (ε = 110), 506 (ε = 33), and 724 nm (ε = 52) and had no EPR features in perpendicular-mode. The solution effective magnetic moment was 3.2 μ_B, supporting an S = 1 spin ground state [47]. The FTIR spectrum of $NMe_4[Ni^{II}MST(OH_2)]$, recorded as a Nujol mull, revealed a peak at 3241 cm^{-1} that is assigned to the O–H vibration from the aqua ligand [37,38].

3.3. Solid-state molecular structure of $[Ni^{II}H_3buea(OH)]^{2-}$ and $[Ni^{II}MST(OH_2)]^-$

The molecular structure of $[Ni^{II}H_3buea(OH)]^{2-}$ was determined by X-ray diffraction methods and the thermal ellipsoid diagram of the complex is shown in Fig. 2A, with selected metrical parameters shown in Table 1. The $[Ni^{II}H_3buea(OH)]^{2-}$ complex crystallized as a monomer, with trigonal bipyramidal (tbp) coordination geometry. The N_4O primary

coordination sphere around the Ni^{II} center is defined by a trigonal plane derived from three deprotonated urea nitrogen atoms with the amine nitrogen and the oxygen atoms from the exogenous hydroxido ligand occupying the axial positions.

The complex shows a distortion from idealized tbp geometry based on the structural parameter $\tau_5 = 0.81$, in which an ideal tbp geometry has $\tau_5 = 1$ and ideal square pyramidal geometry has $\tau_5 = 0$ [52]. This distortion is partially caused by the Jahn-Teller effect that should be present in a high-spin d_8 metal complex having local C_3 symmetry [53]. Another possible contributor to this distortion is the presence of intramolecular H-bonds formed between the urea hydrogen atoms of $[H_3buea]^{3-}$ and O-atom from the Ni^{II}–OH unit. Two relatively short H-bonds are formed as gauged by the N···O distances: N6···O1 and N7···O1 distance of 2.789(1) and 2.786(1) Å that are statistically shorter than the N5···O1 distance of 2.829(1) Å. All three interactions may be considered H-bonds because the N···O distances are under 3.07 Å. However, the two shorter distances are in the region often associated with strong H-bonding [54] and could reflect the fact that the hydroxido ligand only has two available lone pairs.

To our knowledge, the molecular structure of $[Ni^{II}H_3buea(OH)]^{2-}$ represents only the third example of a structurally characterized, 5-coordinate monometallic Ni^{II}–OH. Riordan was the first report such a species but this Ni^{II}–OH complex has a square planar primary coordination sphere coordination with a τ_5 value of 0.0 [22]. Levy's nickel-hydroxido complex has a τ_5 value of 0.86, and is thus the only other Ni^{II}–OH complex with tbp geometry [23]. The Ni1–O1 distance of 2.018(1) Å is significantly longer in $[Ni^{II}H_3buea(OH)]^{2-}$ than in either Riordan's or Levy's complexes, which have Ni1–O1 distances of 1.955(2) and 1.911(4) Å, respectively. This difference is because $[H_3buea]^{3-}$ contains anionic N donors and contains intramolecular H-bonds to the hydroxido ligand, both of which are absent in the other complexes.

The molecular structure of $[Ni^{II}MST(OH_2)]^{-}$ was also determined by X-ray diffraction methods (Fig. 2B, Table 1). The $[Ni^{II}MST(OH_2)]^{-}$ complex crystallized as a monomer, with the N_4O donors around the Ni^{II} center adopting a tbp primary coordination sphere. The three deprotonated sulfonamido nitrogen atoms define the trigonal plane with the amine nitrogen atom and the oxygen atom from the exogenous aqua ligand occupying the apical positions. The complex shows a slight distortion from tbp geometry based on the structural parameter $\tau_5 = 0.86$. As with $[Ni^{II}H_3buea(OH)]^{2-}$, this distortion is expected to be caused by a combination of Jahn-Teller effect and the intramolecular H-bonding network that surrounds the Ni^{II}–OH_2 unit. Two H-bonds are formed between the aqua ligand to the sulfonamido oxygen atom on two of the ligand arms, as gauged by the O···O atom distances of 2.686(2) and 2.679(2) Å.

Five-coordinate terminal Ni^{II}–OH_2 complexes are rare, with the majority of such complexes have τ_5 values closer to 0.0 and thus have distorted square pyramidal primary coordination spheres. To the best of our knowledge, $[Ni^{II}MST(OH_2)]^{-}$ has the the highest τ_5 value of 5-coordinate terminal Ni^{II}–OH_2 complexes and is therefore the closest to having tbp coordination geometry. For comparison, the N-methyl-1,4-diazabicyclo[2.2.2]octane based complex of Stucky [24] and the scorpionate based complex of Yap [55] have τ_5 values of

0.73 and 0.66, representing higher limits for τ_5 values. The Ni1–O1 distance of 2.074(1) Å is shorter in $[Ni^{II}MST(OH_2)]^-$ than in either Stucky's or Yap's complexes, which have Ni1–O1 distances of 2.100(6) and 2.092(2) Å respectively. This difference is also attributed to the presence of intramomolecular H-bonds involving the aqua ligand.

3.4. Electrochemical properties of $[Ni^{II}H_3buea(OH)]^{2-}$ and $[Ni^{II}MST(OH_2)]^-$

The CV of $K_2[Ni^{II}H_3buea(OH)]$ in a 0.1 M TBAP solution in DMF (Fig. 3A) showed an irreversible oxidative event at −830 mV versus $[FeCp_2]^{+/0}$. In addition, the CV for $NMe_4[Ni^{II}MST(OH_2]$ measured in a 0.1 M TBAP solution in CH_2Cl_2 showed a quasi-reversible one-electron oxidation event at +370 mV versus $[FeCp_2]^{+/0}$ (Fig. 3B). This positive shift in redox potential for the complex made with $[MST]^{3-}$ versus analogous $[H_3buea]^{3-}$ complex is expected, as the sulfonamido N atoms on $[MST]^{3-}$ are weaker donors to the metal center than the ureido N atoms [56]. Moreover, the $[Ni^{II}MST(OH_2)]^-$ complex is a mono-anion while the $[Ni^{II}H_3buea(OH)]^{2-}$ is a di-anion, and thus $[Ni^{II}MST(OH_2)]^-$ should be more difficult to oxidize. These results suggested that the Ni^{II} complexes could be oxidized to Ni^{III} species and attempts to chemically prepare these oxidized products were undertaken.

3.5. Preparation and characterization of a Ni^{III} species with $[H_3buea]^{3-}$

The addition of elemental iodine (I_2) to a sample of $K_2[Ni^{II}H_3buea(OH)]$ in DMF resulted in an immediate color change from yellow-green to purple-red. Monitoring this reaction with UV-vis spectroscopy at room temperature showed the growth of an intense peak at λ_{max} = 326 nm ($\varepsilon \sim 2000$) and a peak at λ_{max} = 502 nm ($\varepsilon \sim 570$) (Fig. 4A). The perpendicular-mode EPR spectrum collected at 10 K of the purple-red solution contained a rhombic EPR signal with *g*-values at 2.29, 2.17, and 2.04 (Fig. 4B). This spectrum is consistent with a complex containing a d_7 Ni^{III} center with an S=1/2 spin ground state.[50,57,58] Nearly identical EPR spectra were obtained when the oxidation of $K_2[Ni^{II}H_3buea(OH)]$ was performed in DMA, MeCN, and THF, or when ferrocenium was used as the oxidant.

The Ni^{III} species derived from $[Ni^{II}H_3buea(OH)]^{2-}$ is unstable at room temperature and reacts further to form an EPR silent species. This reaction followed first-order kinetics with respect to the Ni^{III} species in DMF and a half-life of 10 h was determined for the oxidized species at 25 °C. The Ni^{III} species is more stable at lower temperatures: solution samples stored at −30°C retained their rhombic EPR spectra even after several months. In addition, this oxidized product was also stable in the solid state and could be stored under an inert atmosphere at room temperature. Attempts at crystallizing the Ni^{III} species at −80 °C, −30 °C, and room temperature were unsuccessful, with only light yellow powders being isolated. UV-vis spectra of this species indicated that it was not $[Ni^{II}H_3buea(OH)]^{2-}$. ^{1}H-NMR spectra of the powder revealed was nearly identical to that of H_6buea, suggesting some amount of the ligand precursor was present. The oxidized Ni^{III} species also does not reconvert to $[Ni^{II}H_3buea(OH)]^{2-}$ upon reduction. Treating the Ni^{III} complex immediately after its formation with $CoCp_2$ led to a product that had different optical properties to those of $[Ni^{II}H_3buea(OH)]^{2-}$. We also probed the reactivity of the Ni^{III} species with external substrates including 9,10-dihydroanthracene (DHA) and xanthene, yet no reaction was observed with these species.

We have previously shown that the one-electron oxidation of $[M^{II}H_3buea(OH)]^{2-}$ complexes (M^{II} = Fe, Mn, Co) produces their corresponding M^{III}–OH analogs [59]. The combined spectroscopic data for the oxidized product of $[Ni^{II}H_3buea(OH)]^{2-}$ does not allow us to make a similar assignment. While our results support the initial formation of a Ni^{III} species, there is no data that confirms that the hydroxido ligand is still coordinated. In particular, the characteristic peaks associated with the O–H vibration have not been observed in the FTIR spectrum. A new peak appears in the FTIR spectrum at 3320 cm^{-1} after oxidation but its shape and energy do not correspond to bands for O–H vibrations we have observed for other M^{III}–OH with this ligand. The energy of this peak is also in the same region we observe signals from H_6buea, suggesting the possibility that the ligand has been protonated, as found from our NMR studies (see above).

3.6. Preparation and characterization of a Ni^{III} species with $[MST]^{3-}$

We have also explored the oxidation of $[Ni^{II}MST(OH_2)]^{-}$ under similar conditions to $[Ni^{II}H_3buea(OH)]^{2-}$. The Ni^{II}–OH_2 complex could be oxidized with [TBPA][PF_6] to induce a clear color change from lime-green to orange. When the reaction was monitored by UV-vis spectroscopy at room temperature, the growth of a peak at λ_{max} = 312 nm (ε > 12000) and shoulders at 440 nm (ε ~ 1200) and 530 nm (ε ~ 550) are observed (Fig. 5A). The perpendicular-mode EPR spectrum (Fig. 5B) at 10 K showed a rhombic signal with g = 2.29, 2.17, and 2.04. Attempts at crystallization yielded only green crystals, which is likely a Ni^{II} species as this compound is perpendicular-mode EPR silent.

The properties of the Ni^{III} species with $[MST]^{3-}$ are similar to that with $[H_3buea]^{3-}$. It reacts further to form an EPR silent species at room temperature, which occurs within hours. Attempts at crystallizing the oxidized species at −80°C, −30°C, and room temperature were also unsuccessful, with only a light yellow powder again being isolated from the reaction mixture. The UV-vis spectrum of this EPR silent species is similar to the original Ni^{II}–OH_2 compound. However, attempts to immediately reduce the putative Ni^{III} species using $CoCp_2$ led to a species that is different from the starting Ni^{II}–OH_2 compound and its formulation is still unknown.

We have previously shown that $[Fe^{III}MST(OH)]^{-}$ is prepared by the one-electron oxidation of $[Fe^{II}MST(OH_2)]^{-}$ [37]. However, as with $[Ni^{II}H_3buea(OH)]^{2-}$, the spectroscopic data for the oxidized product of $[Ni^{II}MST(OH_2)]^{-}$ does not allow us to make a similar, definitive assignment. An O–H vibration at 3463 cm^{-1} was observed for $[Fe^{III}MST(OH)]^{-}$, but a similar feature was not found in FTIR spectra of the oxidized $[Ni^{II}MST(OH_2)]^{-}$. Moreover, we did not observe any further reactivity with the Ni^{III} species with external substrates that would support a high valent Ni–OH species.

4. Summary

This work has described the preparation and characterization of $K_2[Ni^{II}H_3buea(OH)]$ and $NMe_4[Ni^{II}MST(OH_2)]$, complexes containing terminal Ni^{II}–OH and Ni^{II}–OH_2 moieties. These complexes adopt a distorted tbp geometry as determined by the τ_5 value, which is an uncommon geometry for these types of complexes. Both of these complexes were oxidized by one-electron oxidants to form high-valent Ni^{III} species, as determined by perpendicular-

mode EPR spectroscopy. Both oxidation reactions revealed rhombic perpendicular-mode EPR spectra at 10 K, consistent with an S = 1/2 spin-state derived from a low-spin Ni^{III} metal center. These Ni^{III} species were characterized by UV-vis spectroscopy, EA, and FTIR spectroscopy, but crystals have yet to be grown for either compound. Moreover, the lack of detectable vibration peaks for $Ni^{III}O$–H bonds prevents the definitive assignment of these complexes as high valent Ni–hydroxido species.

Supplementary Material

Refer to Web version on PubMed Central for supplementary material.

Acknowledgments

The authors than the National Institutes of Health, USA (GM050781).

References

1. Du Bois J, Mizoguchi TJ, Lippard SJ. Coord Chem Rev. 2000; 200–202:443.
2. Merkx M, Kopp DA, Sazinsky MH, Blazyk JL, Müller J, Lippard SJ. Angew Chemie Int Ed. 2001; 40:2782.
3. Que L Jr, Tolman WB. Angew Chemie Int Ed. 2002; 41:1114.
4. Hikichi S, Yoshizawa M, Sasakura Y, Akita M, Moro-oka Y. J Am Chem Soc. 1998; 120:10567.
5. Hikichi S, Yoshizawa M, Sasakura Y, Komatsuzaki H, Moro-oka Y, Akita M. Chem - A Eur J. 2001; 7:5011.
6. Mandimutsira BS, Yamarik JL, Brunold TC, Gu W, Cramer SP, Riordan CG. J Am Chem Soc. 2001; 123:9194. [PubMed: 11552841]
7. Benson DE, Haddy AE, Hellinga HW. Biochemistry. 2002; 41:3262. [PubMed: 11863465]
8. Itoh S, Bandoh H, Nakagawa M, Nagatomo S, Kitagawa T, Karlin KD, Fukuzumi S. J Am Chem Soc. 2001; 123:11168. [PubMed: 11697960]
9. Rodríguez L, Labisbal E, Sousa-Pedrares A, García-Vázquez JA, Romero J, Durán ML, Real JA, Sousa A. Inorg Chem. 2006; 45:7903. [PubMed: 16961383]
10. Biswas R, Kar P, Song Y, Ghosh A. Dalt Trans. 2011; 40:5324.
11. Dixon NE, Riddles PW, Gazzola C, Blakeley RL, Zerner B. Can J Biochem. 1980; 58:1335. [PubMed: 6788353]
12. Jabri E, Carr M, Hausinger R, Karplus P. Science (80-). 1995; 268:998.
13. Lipscomb WN, Sträter N. Chem Rev. 1996; 96:2375. [PubMed: 11848831]
14. Christianson DW, Cox JD. Annu Rev Biochem. 1999; 68:33. [PubMed: 10872443]
15. Christianson DW, Fierke CA. Acc Chem Res. 1996; 29:331.
16. Cámpora J, Palma P, del Río D, Álvarez E. Organometallics. 2004; 23:1652.
17. Cámpora J, Matas I, Palma P, Graiff C, Tiripicchio A. Organometallics. 2005; 24:2827.
18. Adhikari D, Mossin S, Basuli F, Dible BR, Chipara M, Fan H, Huffman JC, Meyer K, Mindiola DJ. Inorg Chem. 2008; 47:10479. [PubMed: 18855380]
19. Huang D, Makhlynets OV, Tan LL, Lee SC, Rybak-Akimova EV, Holm RH. Inorg Chem. 2011; 50:10070. [PubMed: 21905646]
20. Zhang YP, Li WW, Li BX, Mu HL, Li YS. Dalt Trans. 2015; 44:7382.
21. Czerny F, Döhlert P, Weidauer M, Irran E, Enthaler S. Inorganica Chim Acta. 2015; 425:118.
22. Kieber-Emmons MT, Schenker R, Yap GPA, Brunold TC, Riordan CG. Angew Chemie Int Ed. 2004; 43:6716.
23. Prema D, Oshin K, Desper J, Levy CJ. Dalton Trans. 2012; 41:4998. [PubMed: 22407327]
24. Ross FK, Stucky GD. Inorg Chem. 1969; 8:2734.

25. Evans DA, Downey CW, Hubbs JL. J Am Chem Soc. 2003; 125:8706. [PubMed: 12862448]
26. Santillan GA, Carrano CJ. Dalton Trans. 2008:3995. [PubMed: 18648703]
27. Kunishita A, Doi Y, Kubo M, Ogura T, Sugimoto H, Itoh S. Inorg Chem. 2009; 48:4997. [PubMed: 19374371]
28. Powell-Jia D, Ziller JW, DiPasquale AG, Rheingold AL, Borovik AS. Dalt Trans. 2009:2986.
29. Hammes BS, Young VG Jr, Borovik AS. Angew Chemie Int Ed. 1999; 38:666.
30. MacBeth CE, Golombek AP, Young VG Jr, Yang C, Kuczera K, Hendrich MP, Borovik AS. Science (80-). 2000; 289:938.
31. Gupta R, MacBeth CE, Young VG, Borovik AS. J Am Chem Soc. 2002; 124:1136. [PubMed: 11841259]
32. Lacy DC, Gupta R, Stone KL, Greaves J, Ziller JW, Hendrich MP, Borovik AS. J Am Chem Soc. 2010; 132:12188. [PubMed: 20704272]
33. Park YJ, Ziller JW, Borovik aS. J Am Chem Soc. 2011; 133:9258. http://www.journals.cambridge.org/abstract_S0010417500020156. [PubMed: 21595481]
34. Park YJ, Cook SA, Sickerman NS, Sano Y, Ziller JW, Borovik AS. Chem Sci. 2013; 4:717. [PubMed: 24058726]
35. Sano Y, Weitz AC, Ziller JW, Hendrich MP, Borovik AS. Inorg Chem. 2013; 52:10229. [PubMed: 23992041]
36. Lacy DC, Park YJ, Ziller JW, Yano J, Borovik AS. J Am Chem Soc. 2012; 134:17526. [PubMed: 22998407]
37. Cook SA, Ziller JW, Borovik AS. Inorg Chem. 2014; 53:11029. [PubMed: 25264932]
38. Lau N, Ziller JW, Borovik AS. Polyhedron. 2014
39. Pandarus V, Zargarian D. Organometallics. 2007; 26:4321.
40. Anderson TJ, Jones GD, Vicic DA. J Am Chem Soc. 2004; 126:8100. [PubMed: 15225035]
41. Zultanski SL, Fu GC. J Am Chem Soc. 2011; 133:15362. [PubMed: 21913638]
42. Lee WZ, Chiang CW, Lin TH, Kuo TS. Chem - A Eur J. 2012; 18:50.
43. Chiang CW, Chu YL, Chen HL, Kuo TS, Lee WZ. Chem - A Eur J. 2014; 20:6283.
44. Tappmeyer WP, Davidson AW. Inorg Chem. 1963; 2:823.
45. Eberson L, Larsson B, Moberg C, Krautwurst KD, Krogsgaard-Larsen P, Ryhage R, Isaksson R. Acta Chem Scand. 1986; 40b:210.
46. Eberson L, Larsson B. Acta Chem Scand. 1987; 41B:367. [accessed June 4, 2014] http://actachemscand.org/pdf/acta_vol_41b_p0367-0378.pdf.
47. Evans DF. J Chem Soc. 1959:2003.
48. Connelly NG, Geiger WE. Chem Rev. 1996; 96:877. [PubMed: 11848774]
49. MacBeth CE, Hammes BS, Young VG, Borovik AS. Inorg Chem. 2001; 40:4733.
50. Pfaff FF, Heims F, Kundu S, Mebs S, Ray K. Chem Commun (Camb). 2012; 48:3730. [PubMed: 22398975]
51. Ma H, Petersen JL, Young VG, Yee GT, Jensen MP. J Am Chem Soc. 2011; 133:5644. [PubMed: 21438640]
52. Addison AW, Rao TN, Reedijk J, van Rijn J, Verschoor GC. J Chem Soc Dalt Trans. 1984:1349.
53. Sickerman NS, Park YJ, Ng GKY, Bates JE, Hilkert M, Ziller JW, Furche F, Borovik AS. Dalton Trans. 2012; 41:4358. [PubMed: 22334366]
54. Emsley J. Chem Soc Rev. 1980; 9:91.
55. Oseback SN, Shim SW, Kumar M, Greer SM, Gardner SR, Lemar KM, DeGregory PR, Papish ET, Tierney DL, Zeller M, Yap GPA. Dalt Trans. 2012; 41:2774.
56. Bordwell FG. Acc Chem Res. 1988; 21:456.
57. Cho J, Sarangi R, Annaraj J, Kim SY, Kubo M, Ogura T, Solomon EI, Nam W. Nat Chem. 2009; 1:568. [PubMed: 20711413]
58. Xiao Z, Patrick BO, Dolphin D. Inorg Chem. 2003; 42:8125. [PubMed: 14658860]
59. MacBeth CE, Gupta R, Mitchell-Koch KR, Young VG, Lushington GH, Thompson WH, Hendrich MP, Borovik AS. J Am Chem Soc. 2004; 126:2556. [PubMed: 14982465]

Appendix A. Supplementary data

CCDC 1501483 and 1501484 contain the supplementary crystallographic data for $K_2[Ni^{II}H_3buea(OH)]$ and $NMe_4[Ni^{II}MST(OH_2)]$ respectively. These data can be obtained free of charge via http://www.ccdc.cam.ac.uk/conts/retrieving.html, or from the Cambridge Crystallographic Data Centre, 12 Union Road, Cambridge CB2 1EZ, UK; fax: (+44) 1223-366-033; or e-mail: deposit@ccdc.cam.ac.uk. Supplementary data associated with this article can be found, in the online version.

Fig. 1.
The ligands used in this study, (**A**) $[H_3buea]^{3-}$ and (**B**) $[MST]^{3-}$.

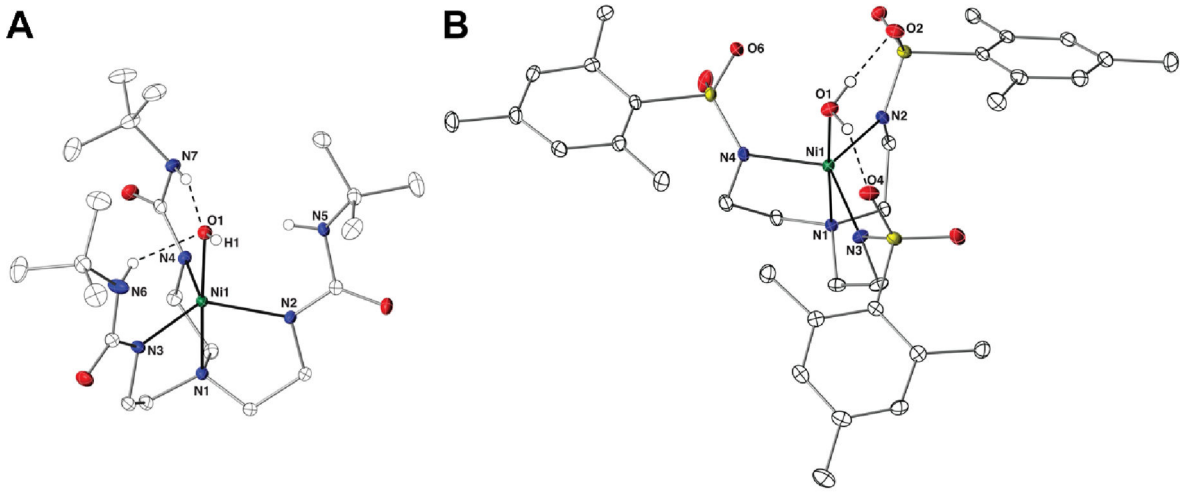

Fig. 2.

Thermal ellipsoid diagram depicting the molecular structure of (**A**) $[Ni^{II}H_3buea(OH)]^{2-}$ and (**B**) $[NiMST(OH_2)]^{-}$. Ellipsoids are drawn at the 50% probability level, and only urea, hydroxido, and aqua H atoms are shown for clarity.

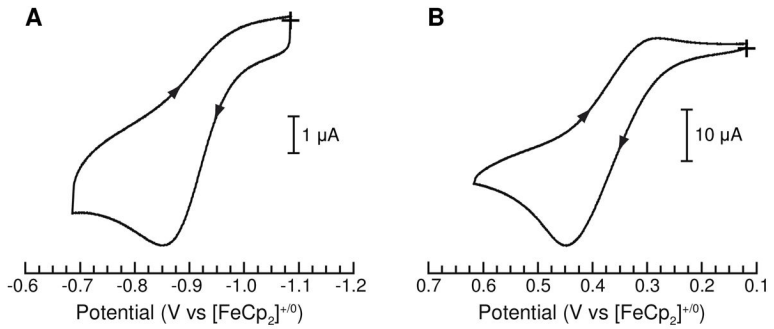

Fig. 3.

Cyclic voltammogram of (**A**) $K_2[Ni^{II}H_3buea(OH)]$, collected at 100 mV s^{-1} in a 0.1 M TBAP solution in DMF using $[CoCp_2]^{0/+}$ as an internal reference, then scaled to $[FeCp_2]^{+/0}$, and of (**B**) $NMe_4[Ni^{II}MST(OH_2)]$, collected at 100 mV s^{-1} in a 0.1 M TBAP solution in CH_2Cl_2 using $[FeCp_2]^{+/0}$ as an internal reference.

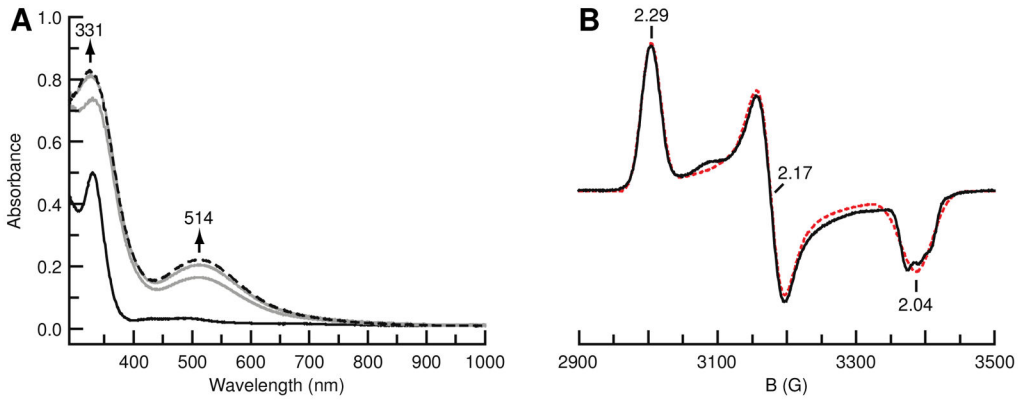

Fig. 4.

(**A**) UV-vis spectrum for oxidation of a 0.4 mM DMF solution of $K_2[Ni^{II}H_3buea(OH)]$ by I_2 at 25 °C, showing the conversion of the initial Ni^{II}–OH species (solid black) to a Ni^{III} species (dashed black) after 5 min. (**B**) Perpendicular-mode X-band EPR spectra taken at 10 K of the putative Ni^{III} species with $[H_3buea]^{3-}$ prepared in DMF with I_2 as the oxidant (solid black) and simulated spectrium (dashed red).

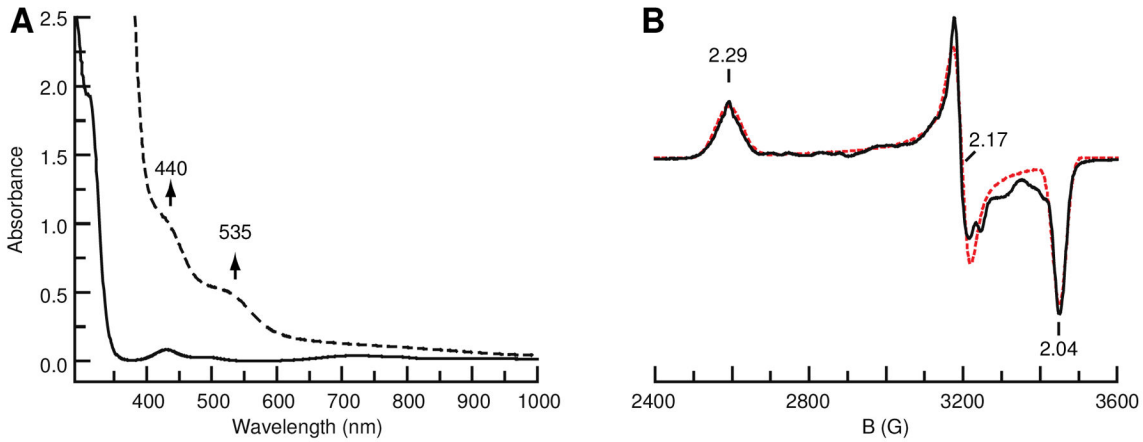

Fig. 5.

(**A**) UV-vis spectrum for oxidation of a 0.4 mM CH_2Cl_2 solution of $NMe_4[Ni^{II}MST(OH_2)]$ by $[TBPA]PF_6$ at 25 °C, showing the conversion of the initial $Ni^{II}–OH_2$ species (solid black) to some Ni^{III} species after 30 s. (**B**) Perpendicular-mode X-band EPR spectra taken at 77 K of the putative Ni^{III} species with $[MST]^{3-}$ prepared in CH_2Cl_2 with $[TBPA]PF_6$ as the oxidant (solid black) and simulated spectrum (dashed red).

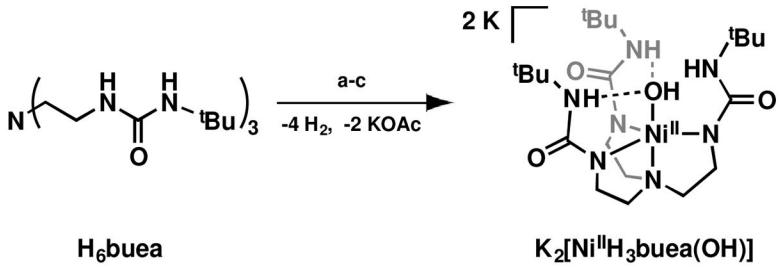

Scheme 1.

Preparation of $K_2[Ni^{II}H_3buea(OH)]$. Conditions (a) 4 KH; (b) $Ni(OAc)_2$; (c) H_2O.

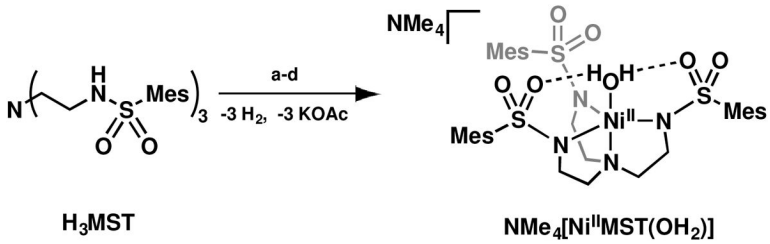

Scheme 2.

Preparation of $NMe_4[Ni^{II}MST(OH_2)]$. Conditions (a) 3 KH, DMA, Ar, rt; (b) $Ni(OAc)_2{\cdot}4H_2O$, DMA, Ar, rt; (c)

Table 1

Selected metrical parameters for $[Ni^{II}H_3buea(OH)]^{2-}$, $[Ni^{II}MST(OH_2)]^{-}$ complexes

	$[Ni^{II}H_3buea(OH)]^{2-}$	$[Ni^{II}MST(OH_2)]^{-}$
	Atomic distances (Å)	
Ni1–O1	2.018(1)	2.074(2)
Ni1–N1	2.106(1)	2.114(2)
Ni1–N2	2.089(1)	2.027(2)
Ni1–N3	2.055(1)	2.051(2)
Ni1–N4	2.059(1)	2.026(2)
Ave. Ni–N_{eq}	2.068(1)	2.035(2)
N5···O1	2.829(1)	
N6···O1	2.789(1)	
N7···O1	2.786(1)	
O1···O2		2.686(2)
O1···O4		2.679(2)
O1···O6		2.998(2)
	Bond angles (°)	
N1–Ni1–O1	177.9(5)	176.8(8)
N1–Ni1–N2	80.5(5)	82.9(8)
N1–Ni1–N3	82.1(6)	82.6(8)
N1–Ni1–N4	83.0(6)	83.8(8)
N2–Ni1–N3	129.1(6)	120.5(9)
N2–Ni1–N4	104.6(5)	109.8(9)
N3–Ni1–N4	120.2(6)	125.4(9)
τ_5 value	0.81	0.86